

Journal of Materials Chemistry A

Accepted Manuscript



This is an *Accepted Manuscript*, which has been through the Royal Society of Chemistry peer review process and has been accepted for publication.

Accepted Manuscripts are published online shortly after acceptance, before technical editing, formatting and proof reading. Using this free service, authors can make their results available to the community, in citable form, before we publish the edited article. We will replace this *Accepted Manuscript* with the edited and formatted *Advance Article* as soon as it is available.

You can find more information about *Accepted Manuscripts* in the [Information for Authors](#).

Please note that technical editing may introduce minor changes to the text and/or graphics, which may alter content. The journal's standard [Terms & Conditions](#) and the [Ethical guidelines](#) still apply. In no event shall the Royal Society of Chemistry be held responsible for any errors or omissions in this *Accepted Manuscript* or any consequences arising from the use of any information it contains.

Cite this: DOI: 10.1039/c0xx00000x

www.rsc.org/xxxxxx

ARTICLE TYPE

Photonic Curing of Aromatic Thiol -ene Click Dielectric Capacitors via Inkjet Printing

Brian Riggs,^{*a} Ravi Elupula^{a,b}, Scott Grayson and Douglas B. Chrisey^a

Received (in XXX, XXX) Xth XXXXXXXXXX 20XX, Accepted Xth XXXXXXXXXX 20XX

DOI: 10.1039/b000000x

Dielectric capacitive energy storage has a wide range of applications such as microelectronic devices, grid scale load leveling, military applications, and personal power supplies. The high charge and discharge rate, along with the high retention and fatigue properties, make dielectric capacitors an attractive means of energy storage. Device manufacturing in industry requires high throughput and high pattern registry printing processes, such as inkjet, that are able to deposit a wide variety of materials. Thiol-alkene systems, [Pentaerythritol tetrakis (3-mercaptopropionate) (PEMP, P), 1,3-Diisopropenylbenzene (DPB, D), 2,4,6-Triallyloxy-1,3,5-triazine (TOTZ, T)] of various compositions were printed via inkjet printing and cured with a xenon flash lamp system. For simplicity, inks were designated PTD0-4, correlating to the amount of DPB in the ink. PTD1-4 demonstrated fluid properties amenable to inkjet printing (with Z factors between 2-11) and were cured to produce mechanically and chemically stable dielectric films. PTD3 showed the best printability and was used for characterization of energy storage. It was found that the dielectric constant varied with curing intensity and energy/voltage. The breakdown strength had no correlation to the curing parameters tested. Weibull analysis of breakdown failure along with dielectric characterization resulted in a volumetric energy density distribution with a peak characteristic energy storage (63% chance of failure) of 32 J/cm³.

Introduction

The past 20 years have seen an enormous increase in demand for high energy density, high power density electric energy storage devices.¹⁻⁶ On the grid scale, instantaneous response to peaks in production or demand require rapid responses in order to stabilize the load which current storage methods, such as Pb-acid or Li-Ion batteries, are unable to keep up with. These fluctuations occur to a greater extent and over longer periods of time in renewable energy sources where energy production heavily relies on meteorological conditions. A major criticism of electric vehicles is the time it takes to recharge the Li-ion battery, which is on the order of hours at home, and at least 30 minutes at supercharge stations. This is the same issue as personal electronics such as smart phones that need to charge overnight to reach full capacity, leading to the necessity of carrying around extra batteries for extended use. Although merely a convenience for personal electronics, fast charging times are crucial for the application of electric vehicles in order to match the effective charge rate of gasoline powered cars. A summary of energy storage materials and their typical performance can be found in Table 1.

Dielectric capacitors are capable of charging within milliseconds and have high fatigue (10⁸ cycles) and retention (90% capacity after 1 month of full charge) properties, making them an attractive method for electrical energy storage. The current

drawback of a dielectric capacitor is that the total gravimetric capacity is being dwarfed by Li-ion batteries by 3 orders of magnitude, requiring significantly greater amounts of material to be used, increasing the cost and weight of any design. Recently, there has been increased attention on the production of high energy density capacitors through the use of high dielectric ceramics,⁷⁻¹⁸ high breakdown polymers,¹⁹⁻³⁰ and composites of those materials.^{5,13,31-38} There have been significant improvements in the development of materials, however, the necessity of large scale manufacturing processes have been overlooked in the pursuit of the largest possible dielectric constants and breakdown fields. In order to have an energy storage system that is practical and economically viable, the materials must be designed with industrial manufacturing in mind.

Table 1: Summary of Modern Energy Storage Materials

Storage Method	Material	Energy Den. (Wh/kg)	Power Den. (W/kg)	Lifetime (cycles)
Super Cap	PANI/Graphene ³⁹	2.4	124000	>1000
Li-ion	LVP/C nanowire ⁴¹	560	*1800	>2000
Capacitor	Polythiourea ²⁰	6.1	*10 ⁶	*10 ⁸
Capacitor	PTD3: This work	9	*10 ⁶	*10 ⁸

*Typical Values

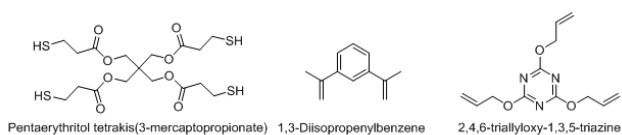


Fig. 1 Chemical structures of the components used in the UV cure inks

Table 2 Prepared solutions for the PTD series of UV cure polymer

	PTD0	PTD1	PTD2	PTD3	PTD4
Thiol:Alkene*	0.26	0.20	0.16	0.13	.010
Mol % DPB	0	40	65	82	95
Mol % TOTZ	84	48	26	11	0
Mol % PEMP	16	12	9	6	5

* Ratio of Thiol functional groups to Alkene functional groups.

Inkjet printing has gained much attention in the past decade due to the drop-on-demand (DOD) delivery system being capable of additive manufacturing on the square meter scale, reducing waste from needless wash steps used in lithographic masking techniques.^{42–49} Inkjet printing is capable of depositing films from 200 nm - 30 μm of polymer solutions or metallic and ceramic nanoparticles.^{10,11,39,42–44,50} The thin film potential of inkjet printing is particular advantageous for high breakdown materials as the dielectric strength increases with decreasing film thickness.

The variety of materials available, as well as the control allotted to the user, enables roll-to-roll (R2R) processing of thin films for dielectrics,^{45,49–52} electrode material,^{45,46,53,54} photovoltaics,^{55–60} and also proteins for bioprinting applications.^{47,49,61} In combination with rapid photonic curing technology, such as xenon flash lamp curing, device production rates can reach up to 100 cm²/min. UV cured materials are especially attractive due to their relatively low energy and high efficiency processes. Ko et al. demonstrated the ease of manufacturing with a thiol alkene based dielectric for transistor gate applications.⁶² Although tested at low voltages, the breakdown strength of their material was promising for dielectric energy storage applications. This paper describes the inkjet printing of an adapted thiol and alkene click polymer cross-linked network onto copper foil substrates polymerized via xenon flash lamp curing for dielectric energy storage applications.

Materials and Methods

Monomer Inks

All monomer solutions were obtained from Sigma Aldrich (St. Louis, MO). Pentaerythritol tetrakis (3-mercaptopropionate) (PEMP) was used as the thiol functionalized monomer. Diisopropenylbenzene (DPB) and 2,4,6 Triallyloxy 1,3,5 Triazine (TOTZ) were the alkene functionalized aromatic compounds. The relative amounts of TOTZ and DPB were varied in order to achieve the printable rheological behavior. Figure 1 shows the chemical structure of all monomers used in the creation of the UV curable inks. Solutions compositions in mole % are listed in Table 2. Each solution were mixed and ultrasonicated for 10 minutes at room temperature to ensure a homogenous solution.

Rheological Characterization and Printing of Capacitors

The Z-factor as expressed by Derby et al.⁴⁴ (Shown in Equation 1) was used to determine the printability of the ink. Viscosity measurements were conducted using a TA parallel plate rheometer with 1° steel cone spindle. Viscosities up to shear rates of 1000 s⁻¹ were measured and viscosity at 10⁵ s⁻¹ was extrapolated in order to more accurately calculate the Z-factor. A hanging drop goniometer was used for surface tension and contact angle measurements.

$$Z = \frac{1}{Oh} = \frac{Re}{\sqrt{We}} = \frac{(\gamma\rho a)^{1/2}}{\eta} \quad (1)$$

In order to control the contact angle on the copper foil, and thereby pattern registry, several different surface treatments were performed including ozone cleaning, ethanol and acetone wipe. Inks were printed using a Fujifilm Dimatix 2800 Inkjet printer with 10 pL (20 μm diameter) print heads. The precise printing parameters (pulse profile, firing voltage, firing frequency) were optimized for each individual ink. Drop spacing varied from 20–40 μm. The drop watcher camera was used to assure that there was minimal satellite drop formation and calculate ejection velocity. The fiduciary camera was used to monitor pattern registry and drop spreading. 1 cm² layers of the PTD inks were printed individually, for cure optimization, and in arrays of 3x5, for high throughput curing demonstration.

Xenon Flash Lamp Curing

The PulseForge 1300 (Novacentrix, Austin, TX) was used to find the optimum curing parameters for the printed films. The fluence and intensity were varied by adjusting the capacitor bank voltage in increments of 50 V. The standard pulse profile is as follows: 450 V, 3000 μs, 5 μp, 50% o.t. (on time). Films were cured in groups of 10 pulses at 1 Hz until they demonstrated mechanical stability through a scratch test. All films were cured after 30 pulses. A multimeter was used to confirm the formation of an electrically insulating layer. Wiping the films with acetone without any material loss demonstrated chemical stability. The optimum cure was defined by chemical, mechanical, and dielectric stability.

Morphological and Chemical Characterization

Optical microscopy was used to inspect for wrinkles, cracks, pinholes, other flaws, and pattern registry. To determine the extent of curing, samples were printed onto KBr substrates and cured at various voltages. These samples were crushed and tested via FTIR for the presence of alkene and thiol functional groups using a Nexus 670 FTIR ESP (Thermo Scientific, Waltham, MA). FTIR spectrums were normalized to the carbonyl peak, which remains at a constant as the carbonyl group is not involved in any reactions. Cured films printed on copper were mounted onto glass slides and cut using a diamond saw for cross sectional SEM to determine material thickness and surface characterization.

Dielectric and Energy Storage Characterization

500 μm diameter gold electrodes were sputtered onto cured polymer films for testing. Dielectric properties were tested using an Agilent 4294a impedance analyzer from 100 Hz-1 MHz using

a two terminal set up. For each set of curing parameters, 4-5 test points were measured. Breakdown measurements were made using Radiant Technologies' (Albuquerque, NM) Premier II Ferroelectric tester with 10 kV amplifier (Trek Inc, Lockport, NY). Breakdown strength was determined by taking leakage current measurements with a 500 ms soak and 1000 ms read time. The voltage was increased according to the sample thickness to obtain a 0.1 MV/cm field increase each loop. Failure was considered when the leakage current of 1 mA was measured. Breakdown measurements were conducted 8-12 times in order to perform a Weibull analysis. The probability of failure as determined by the Weibull analysis was used for energy storage calculations using the linear dielectric energy equation.

$$ED_v = \frac{1}{2} \epsilon_0 \epsilon_r E_b^2 \quad (2)$$

Results and Discussion

Printing of Precursor Inks

The results of the rheological characterization are summarized in Table 3. As DPB is less viscous than PEMP and TOTZ, there is a steady shift to lower viscosities as the concentration is increased. The surface energy of the inks remained constant throughout the composition change. The calculation of the Z-factor was used to guide the optimization of the printing parameters. All inks falling within the Z-factor range of 1-12 were able to print. PTD 0 was too viscous to be ejected from the print head. Figure 2 shows the measured Z factors on a plot of printable Weber and Reynolds numbers. The dashed lines were drawn using the relation $We = (Re/Z)^2$ derived from the Z-factor equation (Equation 1) where $Z=1$ and 10 . The firing voltage was adjusted to form single drops with minimal satellite drop formation. All inks were printed onto copper foil substrates at room temperature using 5 kHz firing frequency with a 3 stage waveform shown in Figure 3. The firing voltages were 31V, 36V, 24V, 20V for PTD1-4 respectively. Figure 4 shows a still frame of an ejected PTD3 drop showing single, coherent drops with elongated tails with a velocity of 8.8 m/s. Nozzle 2 failed to print due to a minor obstruction that occurs during long print runs. These are cleared during printing through a spit, blot cleaning cycle. Figure 5 shows the patterns printed for PTD1, 2, 3, and 4. 1 cm squares were chosen for simplicity and offered enough area to do the required characterization (chemical, structural and energy storage). Optical analysis of print registration showed that there was a 1 mm spreading from the initial pattern. Printing small arrays of capacitor films (3 x 5 arrays) allowed for high throughput testing of a wide range of curing parameters. From the initial screening, it was determined that the films required a minimum of 30 pulses at 4.2 kW/cm² and 5 J/cm² in order to have a mechanically and chemically stable film. The upper limit of curing was set at 1 pulse at 14 kW/cm² and 10 J/cm² at which point the monomer ink would evaporate and burn. Based off of print and cure testing, it was determined that PTD3 would be used for the remainder of the dielectric and energy storage characterization. The fluid properties, as well as surface interactions with copper, allowed it to consistently print with little spreading or deformation. It was noted that PTD4 would separate over long prints leaving a macroscopic compositionally heterogeneous print while PTD1

and 2 didn't maintain proper pattern registry.

Chemical and Morphological Analysis

FTIR for PTD3 cured at different voltages can be found in Figure 6. Scans were normalized to the carbonyl peak at 1746 cm⁻¹ as it is non-reacting. The reduction and elimination of the alkene and thiol peaks at 3100 cm⁻¹ and 2550 cm⁻¹ respectively demonstrate that the thiol alkene click reaction ran to completion, resulting in a completely cross-linked polymer with no excess dangling bonds. Due to the skew in stoichiometry, thiol was found to be deficient, which allowed it to easily react to completion with the available alkene groups. As seen however, the alkene group disappears when cured at 600V.

Table 3 Fluid Characterization and calculation of Printability

	Viscosity (cP)	Surface Tension (mN/m)	Density (g/cm ³)	Z-factor
PTD0	39	30	1.24	0.73
PTD1	12	30	1.03	2.17
PTD2	5.4	30	0.98	4.70
PTD3	4.1	30	0.94	6.07
PTD4	2.28	30	0.93	10.86

.Bolded Z-factors fall within the printable range

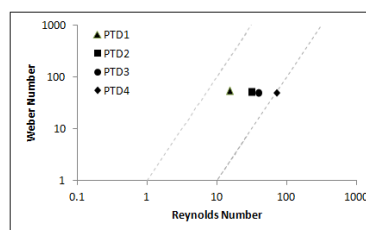


Fig. 2 Plot of printable Weber and Reynolds number for inkjet printing. The dashed lines represent the Z factors 1 and 10. The plotted data shows the Z factors for PTD1-4



Fig. 3 Waveform used for printing dielectric monomer inks

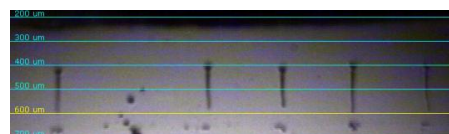


Fig. 4 Still frame from *in situ* camera for PTD3 drops being ejected from the print head. Drops remain cohesive with 350 μm tails.

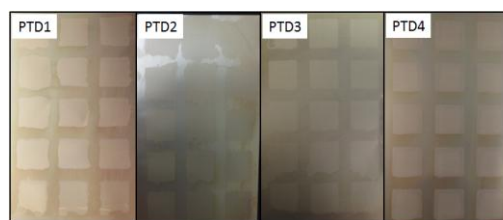


Fig. 5 Printed arrays of 1 cm squares of PTD1-4. PTD1 and 2 shows minor deformation of pattern registry during curing. PTD4 shows minor separation of ink components during long prints. PTD3 shows minor misprints due to satellite drops.

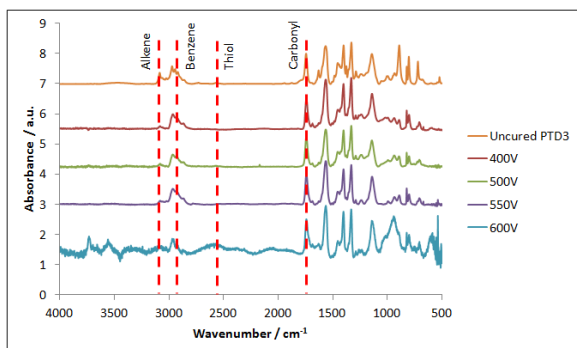


Fig. 6 FTIR results from cured PTD3 printed capacitor films

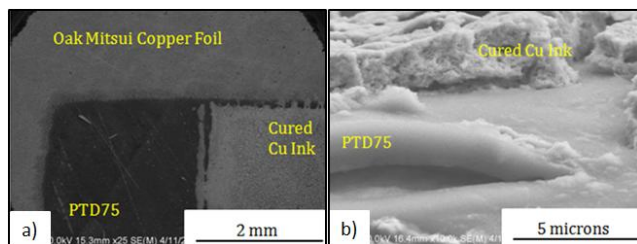


Fig. 7 a) Surface image of PTD3 cured onto copper foil with a printed copper top electrode b) cross section of PTD3 showing fully dense polymer film

This would suggest that the alkene groups are able to activate and bond without the need of thiol radical production at high energies, which are not available in conventional UV processing techniques that have power in the 100 mW range.

Figure 7 shows SEM images of the printed layers. Figure 7(a) shows the surface morphology of the printed films printed onto copper foils with a printed copper top electrode. The differentiation between insulating and conducting layers are obvious due to the contrast within the image. The minor scratches on the surface of PTD75 are due to in line connectivity and chemical stability testing. Figure 7(b) shows the cross section that was used for thickness measurements and characterization of the interior film morphology. The film is fully dense as is characteristic of typical polymer network films. The average film thickness was measured to be 1.6 microns.

Dielectric and Energy Storage Properties

The effects of curing energy and intensity were examined by varying the discharge voltage. With a set pulse width (3000 μ s) increasing the discharge voltage increases the peak intensity as well as the overall energy the material is exposed to. As seen in the FTIR studies, this can affect the total number of bonds formed and thereby the extent of cross-linking. These morphological and chemical differences would also cause a change in dielectric and energy storage properties. Figure 8a shows the frequency dependent dielectric constant for all curing conditions. All curing conditions show <10% loss up to 100 kHz. The dielectric constant also has a 5% drop from 100 Hz to 1 MHz making it viable for a wide range of frequency applications. Figure 8b shows the change of dielectric constant with curing voltage for PTD3. There is a peak in performance at 450V with a dielectric constant of 21. As shown previously in Figure 6, the material is not fully bonded until 600V. This leads to the conclusion that left

over alkene bonds contribute to the dielectric constant. Within DPB the alkene and methyl arm have a minor polarity. It is proposed that when the alkene group does not bond with a thiol, the methyl-alkene arm is allowed to rotate to align with the changing field, contributing to the dielectric constant. With increased curing voltage the alkene arms are bonded into the network, preventing the rotational dipole from contributing to the dielectric constant. From 400V to 450V there was a increase in dielectric constant. This was discussed in another paper examining the separate effects of curing intensity and fluence on PTD0.⁶³ It was argued that at constant intensity, increasing the fluence provides a rapid, full cure freezing structural dipoles, such as hydrogen carbonyl attraction, into place. The increase from 400V to 450V would follow this trend as well. In the PTD series of polymers there is a competition between the dielectric constant provided by free alkene arms and the dipole created by the carbonyl-hydrogen attraction. At 450V, this is balanced to find the maximum dielectric constant.

As dielectric breakdown is a stochastic phenomenon, a Weibull plot (Figure 9) is used for analysis where alpha and beta represent the scale and shape parameter respectively. The shape parameter determines the tightness of failure cluster. Higher values of the

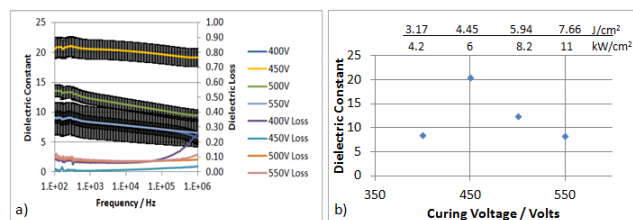


Fig. 8 a) Frequency dependence of dielectric constant and loss for PTD3 cured at different voltages. b) Dielectric constant at 1 kHz for samples cured at discharge voltages of 400-550V. The label at the top outlines the intensity and fluence for each curing voltage

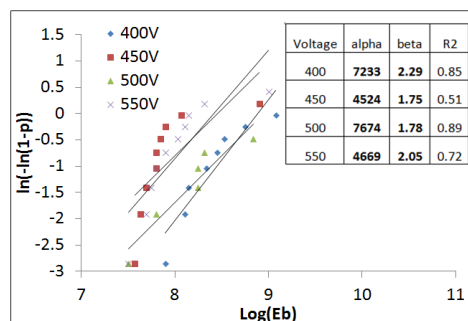


Fig. 9 Weibull analysis for PTD4 at multiple curing voltages

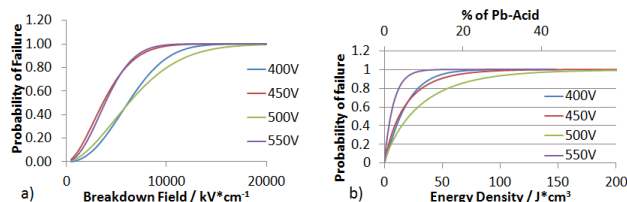


Fig. 10 a) Weibull distribution of the breakdown field for PTD3 at different curing voltages. b) Weibull distribution of volumetric energy density based off the dielectric constant at 1 kHz and the Weibull distribution of breakdown in a)

shape parameter indicates that there is less variation in the breakdown strength. The scale parameter is the field at which there is a 63% chance of failure and is called the characteristic breakdown field. This was used for calculating the volumetric energy density. The full Weibull distribution of failure can be found in Figure 10a. This shows the probability of failure for all possible fields up to 100% chance of failure. It can be seen from the table inset of Figure 9 and Figure 10a that there is no correlation between dielectric strength and the curing voltage. Figure 10b shows the probability of failure for all possible volumetric energy densities up until 100% failure. The energy density was calculated using the linear dielectric capacitor energy equation (Equation 2) with the Weibull distribution as the breakdown field and the dielectric constant measured at 1 kHz as previously shown. The two most interesting curing voltages are the 450V and 400V samples. With characteristic breakdown fields and dielectric constants respectively of 4524 kV/cm and 21 and 7233 kV/cm and 8, their energy density distributions overlap for most of the distribution. This is due to the balance of dielectric constant and breakdown strength in calculating the total energy storage of the device. Optimally both a high dielectric constant and breakdown field are desired as to maximize the total energy storage. The sample cured at 500V shows the best energy storage distribution with a breakdown strength of 7674 kV/cm, dielectric constant of 13 and characteristic volumetric energy storage of 32 J/cm³.

Conclusion

High energy density thiol-ene polymer networks were printed and photonicallly cured to demonstrate large-scale production of dielectric energy storage materials. All PTD solutions had fluid properties amenable to inkjet printing however PTD3 showed the least spreading and separation over time making it the most attractive for large-scale production and industrial application. The low loss (<10%), high dielectric constant (>10), and high breakdown fields make the PTD series attractive for printed electronic applications such as microelectronics, personal electronics, and grid scale applications. It was shown that photonic curing through xenon flash lamp exposure enable large scale curing to compliment the deposition method allowing for rapid production (<5 minutes) of a large number (40) of devices. The technology used during this research already exists on the industrial scale, allowing PTD3 to be quickly adopted into commercial and industrial applications. The high intensity and fluence of the photonic curing process has a distinct effect on the energy storage properties of the PTD3 films due to the change of structure during the curing process. The dielectric constant showed variation with curing voltage with a peak at 450V. There was no correlation with curing voltage and breakdown strength. The thin polymer film capacitors demonstrated high breakdown strengths (>7 MV/cm) and high dielectric constant (13) leading to a high energy density (32 J/cm³, 9 Wh/kg, or 10% of Pb-acid batteries).

Acknowledgements

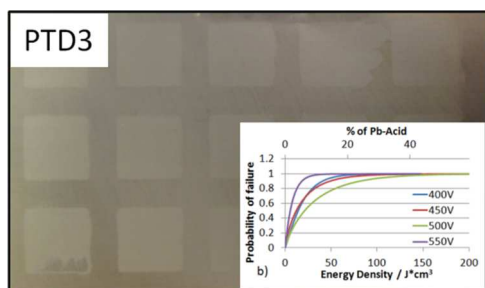
This work was conducted under the NSF-EFRI-RESTOR #1038272.

References

1. A. V Wagner, G. W. Johnson, and T. W. B. Jr, 1999.
2. B. Lawrence, University of Missouri-ROLLA, 2001.
3. X.-Z. Chen, Z.-W. Li, Z.-X. Cheng, J.-Z. Zhang, Q.-D. Shen, H.-X. Ge, and H.-T. Li, *Macromol. Rapid Commun.*, 2011, **32**, 94–9.
4. E. P. Gorzkowski, M.-J. Pan, B. Bender, and C. C. M. Wu, *J. Electroceramics*, 2007, **18**, 269–276.
5. P. Barber, S. Balasubramanian, Y. Anguchamy, S. Gong, A. Wibowo, H. Gao, H. J. Ploehn, and H.-C. zur Loye, *Polymer Composite and Nanocomposite Dielectric Materials for Pulse Power Energy Storage*, 2009, vol. 2.
6. C. Liu, F. Li, L.-P. Ma, and H.-M. Cheng, *Adv. Mater.*, 2010, **22**, E28–62.
7. G. Arlt, D. Hennings, and G. de With, *J. Appl. Phys.*, 1985, **58**, 1619.
8. H. Y. Lee, K. H. Cho, and H.-D. Nam, *Ferroelectrics*, 2006, **334**, 165–169.
9. M. Tio, C. Capacitors, B. Kim, T. Park, and M. Kim, *J. Korean Phys. Soc.*, 1998, **32**, 289–292.
10. X. Zhao, J. R. G. Evans, M. J. Edirisinghe, and J. H. Song, *Ceram. Int.*, 2003, **29**, 887–892.
11. S. Nam, S. Lee, and Y. Lee, *J. Ceram. Process. Res.*, 2008, **9**, 6–9.
12. R. A. Islam and S. Priya, *J. Am. Ceram. Soc.*, 2006, **89**, 3147–3156.
13. Z. Yue, X. Wang, and L. Zhang, *J. Mater. Sci. Lett.*, 1997, **6**, 9–11.
14. T. M. Kamel and G. de With, *J. Eur. Ceram. Soc.*, 2008, **28**, 851–861.
15. P. Ren, H. Fan, X. Wang, and K. Liu, *Int. J. Appl. Ceram. Technol.*, 2012, **9**, 358–365.
16. F. Gao, X. Donf, C. Mao, F. Cao, and G. Wang, *J. Am. Ceram. Soc.*, 2011, **94**, 4162–4164.
17. D. Yi, J. Yuan, H. Liu, Y. Shen, Y.-H. Lin, C.-W. Nan, X. Xi, and J. He, *J. Electroceramics*, 2012, **29**, 95–98.
18. S. Jiang, L. Zhang, G. Zhang, S. Liu, J. Yi, X. Xiong, Y. Yu, J. He, and Y. Zeng, *Ceram. Int.*, 2013, **39**, 5571–5575.
19. Z. Ahmad, in *Dielectric Material*, 2012, pp. 3–26.
20. Q. Burlingame, S. Wu, M. Lin, and Q. M. Zhang, *Adv. Energy Mater.*, 2013, n/a–n/a.

21. B. Chu, X. Zhou, B. Neese, and Q. M. Zhang, *IEEE Trans. Dielectr. Electr. Insul.*, 2006, **13**, 1162–1169.
22. I. Ishino, M. Hikita, Y. Suzuki, T. Mizutani, and M. Ieda, *Electr. Eng. Japan*, 1992, **112**, 1–10.
23. M. Li, N. Stingelin, J. J. Michels, M.-J. Spijkman, K. Asadi, K. Feldman, P. W. M. Blom, and D. M. de Leeuw, *Macromolecules*, 2012, **45**, 7477–7485.
24. M. Meunier and N. Quirke, *J. Chem. Phys.*, 2000, **113**, 369.
25. S.-J. Park, K.-S. Cho, and S.-H. Kim, *J. Colloid Interface Sci.*, 2004, **272**, 384–90.
26. G. T. Pawlikowski, in *MRS Spring Meeting*, 2009, vol. 1156.
27. M. Rabuffi and G. Picci, *IEEE Trans. Plasma Sci.*, 2002, **30**, 1939–1942.
28. M. Rahimabady, K. Yao, S. Arabnejad, L. Lu, V. P. W. Shim, and D. Cheong Wun Chet, *Appl. Phys. Lett.*, 2012, **100**, 252907.
29. Y. Wang, X. Zhou, M. Lin, and Q. M. Zhang, *Appl. Phys. Lett.*, 2009, **94**, 202905.
30. S. Wu, W. Li, M. Lin, Q. Burlingame, Q. Chen, A. Payzant, K. Xiao, and Q. M. Zhang, *Adv. Mater.*, 2013, **25**, 1734–8.
31. R. Popielarz, C. K. Chiang, R. Nozaki, and J. Obrzut, *Macromolecules*, 2001, **34**, 5910–5915.
32. M. Arbatti, X. Shan, and Z.-Y. Cheng, *Adv. Mater.*, 2007, **19**, 1369–1372.
33. R. Popielarz and C. K. Chiang, *Mater. Sci. Eng. B*, 2007, **139**, 48–54.
34. Y. Zhou, Q. Zhang, J. Luo, Q. Tang, and J. Du, *Scr. Mater.*, 2011, **65**, 296–299.
35. Y. Bai, Z.-Y. Cheng, V. Bharti, H. S. Xu, and Q. M. Zhang, *Appl. Phys. Lett.*, 2000, **76**, 3804.
36. P. Barber, P. J. Pellechia, H. J. Ploehn, and H.-C. zur Loye, *ACS Appl. Mater. Interfaces*, 2010, **2**, 2553–9.
37. T. Zhou, J.-W. Zha, R.-Y. Cui, B.-H. Fan, J.-K. Yuan, and Z.-M. Dang, *ACS Appl. Mater. Interfaces*, 2011, **3**, 2184–8.
38. V. S. Puli, R. Elupula, B. C. Riggs, S. M. Grayson, R. S. Katiyar, and D. B. Chrisey, *Int. J. Nanotechnol.*, 2014, **in Press**.
39. Y. Xu, I. Hennig, D. Freyberg, A. James Strudwick, M. Georg Schwab, T. Weitz, and K. Chih-Pei Cha, *J. Power Sources*, 2014, **248**, 483–488.
40. Z. Zhang, G. Wang, Y. Li, X. Zhang, N. Qiao, J. Wang, J. Zhou, Z. Liu, and Z. Hao, *J. Mater. Chem. A*, 2014.
41. Q. Wei, Q. An, D. Chen, L. Mai, S. Chen, Y. Zhao, K. M. Hercule, L. Xu, A. Minhas-Khan, and Q. Zhang, *Nano Lett.*, 2014, **14**, 1042–8.
42. R. I. Tomov, M. Krauz, J. Jewulski, S. C. Hopkins, J. R. Kluczowski, D. M. Glowacka, and B. a. Glowacki, *J. Power Sources*, 2010, **195**, 7160–7167.
43. N. Ramakrishnan, P. K. Rajesh, P. Ponnambalam, and K. Prakasan, *J. Mater. Process. Technol.*, 2005, **169**, 372–381.
44. B. Derby, *J. Eur. Ceram. Soc.*, 2011, **31**, 2543–2550.
45. J. Lim, J. Kim, Y. J. Yoon, H. Kim, H. G. Yoon, S.-N. Lee, and J. Kim, *Int. J. Appl. Ceram. Technol.*, 2012, **9**, 199–205.
46. B.-J. de Gans, P. C. Duineveld, and U. S. Schubert, *Adv. Mater.*, 2004, **16**, 203–213.
47. B. Derby, *J. Mater. Chem.*, 2008, **18**, 5717.
48. B.-J. de Gans and U. S. Schubert, *Langmuir*, 2004, **20**, 7789–93.
49. M. Singh, H. M. Haverinen, P. Dhagat, and G. E. Jabbour, *Adv. Mater.*, 2010, **22**, 673–85.
50. R. C. Pullar, Y. Zhang, L. Chen, S. Yang, J. R. G. Evans, P. K. Petrov, A. N. Salak, D. a. Kiselev, A. L. Kholkin, V. M. Ferreira, and N. M. Alford, *J. Eur. Ceram. Soc.*, 2007, **27**, 4437–4443.
51. J. Wang and J. R. G. Evans, *J. Comb. Chem.*, 2005, **7**, 665–72.
52. W. Clemens, W. Fix, J. Ficker, a. Knobloch, and a. Ullmann, *J. Mater. Res.*, 2011, **19**, 1963–1973.
53. Y. Sakai, T. Futakuchi, and M. Adachi, *Jpn. J. Appl. Phys.*, 2008, **47**, 7630–7634.
54. J. Perelaer, P. J. Smith, D. Mager, D. Soltman, S. K. Volkman, V. Subramanian, J. G. Korvink, and U. S. Schubert, *J. Mater. Chem.*, 2010, **20**, 8446.
55. S. H. Eom, S. Senthilarasu, P. Uthirakumar, S. C. Yoon, J. Lim, C. Lee, H. S. Lim, J. Lee, and S.-H. Lee, *Org. Electron.*, 2009, **10**, 536–542.
56. S. E. Shaheen, D. S. Ginley, G. E. Jabbour, and G. Editors, 2005, **30**, 10–19.
57. J. Jung, D. Kim, J. Lim, C. Lee, and S. C. Yoon, *Jpn. J. Appl. Phys.*, 2010, **49**, 05EB03.
58. C. N. Hoth, P. Schilinsky, S. A. Choulis, and C. J. Brabec, 2008.
59. P. Calvert, *Chem. Mater.*, 2001, **13**, 3299–3305.
60. C. N. Hoth, S. a. Choulis, P. Schilinsky, and C. J. Brabec, *Adv. Mater.*, 2007, **19**, 3973–3978.
61. H. Dong, W. W. Carr, and J. F. Morris, *Phys. Fluids*, 2006, **18**, 072102.
62. J. M. Ko, Y. H. Kang, C. Lee, and S. Y. Cho, *J. Mater. Chem. C*, 2013, **1**, 3091.

-
63. B. C. Riggs, R. Elupula, V. S. Puli, S. M. Grayson, and D. B. Chrisey, *MRS Proc.*, 2014, **1630**.



This work ties together the ease of manufacturing through high-throughput techniques and materials processing while increasing performance from conventional methods.